Catalysis Surveys from Asia (2019) 23:102–109
https://doi.org/10.1007/s10563-019-09269-1

Preparation and Characterization of Carbon Modified Pd-Cu/Palygorskite for Room-Temperature CO Oxidation Under Moisture-Rich Conditions

Xiao Li[1] · Yongzhao Wang[1] · Tingting Lv[1] · Yalin Xu[1] · Yongxiang Zhao[1]

Published online: 6 March 2019

Abstract
Pd–Cu/Palygorskite catalysts were prepared by a deposition precipitation method using palygorskite (PC/Pal) and carbon modified palygorskite (PC/Pal-C) as supports, respectively. Their catalytic activities toward CO oxidation at room temperature and in humid circumstances were investigated. It is found that PC/Pal-C exhibits much higher catalytic activity and stability than PC/Pal for room-temperature CO oxidation under moisture-rich conditions. X-ray photoelectron spectroscopy (XPS) and H_2-TPR results indicate that the more active Pd^{2+} and highly dispersed $Cu_2Cl(OH)_3$ species present on the PC/Pal-C, which promotes the higher catalytic activity. The thermogravimetric (TG) and water contact angles (CA) results suggest that the slightly enhanced hydrophobicity of PC/Pal-C could properly restrain the moisture condensation on the catalyst surface, which may account for the excellent catalytic stability. The more surface active species and the proper hydrophobicity may be responsible for the excellent catalytic performance of PC/Pal-C.

Keywords Pd–Cu/Palygorskite · Carbon modified · CO oxidation · Moisture-rich

1 Introduction

Carbon monoxide (CO) is one of most common components in automotive exhaust fumes and industrial waste gases, which is largely harmful to human health and environment. Thus, CO elimination has become the focus of the global scientific community. CO catalytic oxidation has been considered to be an efficient and economical method for the abatement of carbon monoxide emission. Furthermore, low-temperature CO oxidation is of more significant importance, not only with regard to theoretical studies as a model reaction, but also in terms of practical application, such as gas masks, lowering automotive emission and purification of hydrogen for proton exchange membrane fuel cells (PEMFCs), etc [1–6].

Among various catalysts, noble metal catalysts show excellent catalytic activity for CO oxidation at low temperature, but they also have several defects. For example, Au-based catalysts are sensitive to halogen-including compounds and indoor light, leading to the deactivation during the long-time reaction or storage process [7–14]. Non-noble metal oxide and mixed oxide catalysts exhibit prominent catalytic activity at low temperature, especially Co_3O_4 and the Cu-based catalysts [15–20]. Xie et al. [21] reported that Co_3O_4 nanorods showed extraordinarily high activity for CO oxidation even at temperature as low as −77 °C under dry conditions, however, the catalysts seriously deactivated in the company of trace amount of moisture (3–10 ppm) owing to the blocking of active sites by water molecules adsorption. In contrast to metal oxides and supported gold-based catalysts, supported Wacker-type catalysts have been reported to be active and stable for room-temperature CO oxidation in the presence of moisture and organic halides, and the water may participate in CO_2 formation step, whereas the deactivation is inevitable under moisture-rich conditions [22]. Shen et al. [23, 24] prepared Pd–Cu–Cl_x/Al_2O_3 catalysts by a NH_3 coordination-impregnation method, which exhibited

Electronic supplementary material The online version of this article (https://doi.org/10.1007/s10563-019-09269-1) contains supplementary material, which is available to authorized users.

✉ Yongzhao Wang
catalyst@sxu.edu.cn

[1] Engineering Research Center of Ministry of Education for Fine Chemicals, School of Chemistry and Chemical Engineering, Shanxi University, Taiyuan 030006, China

an outstanding catalytic activity for low-temperature CO oxidation. However, during the long process of reaction at high relative humidity, the water vapor in the feed gases was adsorbed and condensed on the catalyst surface due to the strong hydrophilicity of Al_2O_3, which leaded to the aggregation and migration of the Cu species. This weakened the interaction between Pd and Cu species, and Pd^0 species over the surface of the catalyst was hard to re-oxidize back to the Pd^{2+} by copper species, which inhibited the redox cycle and resulted in the decrease of CO oxidation activity under the high moisture reaction conditions. Zhou et al. [25] reported that Pd–Cu–Cl_x/CNT catalysts prepared by the two-step impregnation method exhibited good stability and water-resistance, when the moisture level in the reactant gas was 3.1 vol.% at 25 °C. Nevertheless, the loading of Pd for the catalyst was 3.3%, which was much higher than that reported in other literatures [26, 27]. On the basis of previous work [24, 25, 28], we also found that Pd–Cu/Palygorskite catalysts exhibited the low catalytic activity and poor stability in the presence of high concentration moisture or at high space velocity. Generally, moisture exists inevitably in practical application, and the moisture concentration in the feed gas is usually near-saturated.

Most of researchers [29–32] often use biomass as carbon source to modify palygorskite by hydrothermal method or pyrolysis method, which combines the surface properties of activated carbon with the texture properties of palygorskite. These carbon modified palygorskite materials are usually used in the field of adsorption, decolorization and fuel cell, etc. However, the application in CO catalytic oxidation is rarely reported.

In this paper, a simple process has been developed for the preparation of carbon-modified palygorskite, which was used as a support to prepare Pd–Cu/Palygorskite catalysts by a deposition precipitation method. Compared with the catalyst supported on palygorskite without modification (PC/Pal), the catalyst supported on the carbon modified palygorskite (PC/Pal-C) exhibited excellent catalytic performance for CO oxidation at room temperature and in the presence of high concentration moisture. Herein, PC/Pal-C and PC/Pal were characterized by ICP-AES, TG, XRD, N_2-physisorption, FT-IR, H_2-TPR, XPS and CA, and the relationship between the structure and catalytic performance was also discussed in detail.

2 Experimental

2.1 Materials

Palygorskite is obtained from Anhui Mingmei MinChem Co., Ltd. (Hefei, China), and used without further purification. Besides the H_2O molecules, the primary chemical components of the palygorskite are 64.6 wt% SiO_2, 20.7 wt% Al_2O_3, 13.8 wt% MgO, and it also contains very small amounts of Fe_2O_3 and Mn_3O_4, which are no more than 1 wt%. All of the other chemicals are of analytical grade and purchased from Shanghai Chemical Reagent Co., Ltd. (Shanghai, China).

2.2 Support Modification

1 g of sucrose was dissolved in 20 ml of distilled water, and 10 g of palygorskite was added to the above solution. The solution was stirred until forming slurry. Then the slurry was evaporated to dry, and dried at 90 °C for 3 h. The modified support was obtained after calcining at 350 °C for 3 h in N_2 atmosphere. The palygorskite modified by carbon was designated as Pal-C and the palygorskite without treatment was designated as Pal.

2.3 Catalyst Preparation

The catalysts were prepared by the deposition precipitation method as follows: 0.02 g of $PdCl_2$ and 1.82 g of $CuCl_2{\cdot}2H_2O$ were dissolved in 40 mL of H_2O, and then 5 g of modified support was added into the above solution. The suspension was transferred to a water bath preheated at 70 °C and stirred for 15 min. Following $NH_3{\cdot}H_2O$ was added drop-wise into the suspension until a pH of 7 was reached. The suspension was removed from the water bath and aged for 12 h. After filtration, the samples were dried in air at 80 °C for 3 h and at 120 °C for another 3 h. Finally the dried samples were calcined at 300 °C for 3 h. The obtained sample was designated as PC/Pal-C. The catalyst prepared by the pure palygorskite without modification was denoted as PC/Pal. In both of the two samples, the contents determined by the inductively coupled plasma-atomic emission spectroscopy (ICP-AES) were 0.35 wt% and 12 wt% for Pd and Cu, respectively, which were almost the same as the theoretical values.

2.4 Catalyst Characterization

The contents of Pd and Cu in the catalysts were analyzed with an ICP-AES instrument (710ES, Varian, USA). All determinations were conducted at least in triplicate.

Thermogravimetric analysis (TG) was carried out in N_2/O_2 atmosphere at a heating rate of 10 ℃/min by a thermal analyzer (STA449F3, NETZSCH, Germany).

XRD patterns of the catalysts were recorded using a diffraction spectrometer with CuKα radiation (λ = 0.154 nm) at a scanning rate of 2.4 °/min (D8 Advance, Bruker, Germany).

FT-IR spectra were obtained by a Fourier transform infrared spectrometer (Tensor 27, Bruker, Germany) with pressed

KBr pellets in the range of 400–4000 cm^{-1}. 16 scans were collected for each sample with a resolution of 4 cm^{-1}.

CA was measured on a contact-angle system (OCA20, Dataphysics, Germany) at ambient temperature. The sample was uniformly mounted on double-sided carbon tape, with one side stuck on a glass slide. The distilled water was slowly dropped onto the surface of the carbon tape coated with various samples. Reported CA value is the average of three independent measurements.

Textural analysis was measured at − 196 °C on a N_2-physisorption analyzer (ASAP-2020, Micromeritics, USA). The sample was degassed at 150 °C for 5 h before the adsorption test. The multi-point BET procedure was used to assess the specific surface area (S_{BET}) and the pore volume. The pore size distribution was determined by applying the Barrett–Joyner–Halenda (BJH) method.

H_2-TPR was performed with a chemical adsorption instrument (AutoChemII 2920, Micromeritics, USA). 30 mg of sample was loaded. 5 vol% H_2/N_2 (30 mL/min) mixture was introduced to the sample and the temperature was raised to 700 °C at a rate of 10 ℃/min. The uptake amounts of H_2 were measured by a thermal conductivity detector (TCD), which was calibrated by the quantitative reduction of CuO to the metallic copper.

X-ray photoelectron spectroscopy (XPS) spectra of the catalysts were determined on ESCALAB 250 spectrometer using Al Kα radiation as the excitation source. The C 1s signal (284.8 eV) was used as the reference to correct the binding energies.

2.5 Measurement of Catalytic Performance

The measurements of catalytic activity for CO oxidation at room temperature and in humid circumstances were performed in a fixed-bed continuous flow microreactor. The microreactor was a 8 mm i.d. quartz u-tube, and a thermocouple was set into the catalyst bed to measure the temperature. The samples were sieved to 40–60 mesh so that temperature gradients and pressure drop over the catalyst bed were negligible. 300 mg of catalyst was used for each test. The feed gas adjusted by mass flow controllers consisted of 0.5 vol.% CO, moisture and air for balance, with a space velocity of 8000 h^{-1}. No pretreatment was applied before the catalytic activity test. The quantitative analysis of CO was performed with an on-line gas chromatograph equipped with a 3 m column packed with carbon molecular sieve, a post-column methanator and a flame ionization detector (FID). In order to enhance the sensitivity of the detection, CO and CO_2 were converted to CH_4 by the methanator at 360 °C before entering into the FID. The activity was expressed by CO conversion, which was calculated according to:

$$X(\%) = (CO_{inlet} - CO_{outlet})/CO_{inlet} \times 100$$

where X is the CO conversion, CO_{inlet} represents the initial CO concentration in the inlet, and CO_{outlet} represents the CO concentration in the outlet.

3 Results and Discussion

3.1 TG Analysis

The carbon modification of Pal was confirmed by TG analysis. The mass loss curves for supports and catalysts are shown in Fig. 1. The curves reveal the dehydration/dehydroxylation of palygorskite and the oxidative degradation of carbon species on the surface of palygorskite. The initial weight loss is around 5.3% between 30 °C and 120 °C for the pure Pal, which could be related to the removal of physically adsorbed water molecules. The second mass loss step is originated from the dehydration of residual zeolitic water and partial structural water. The third is observed in the

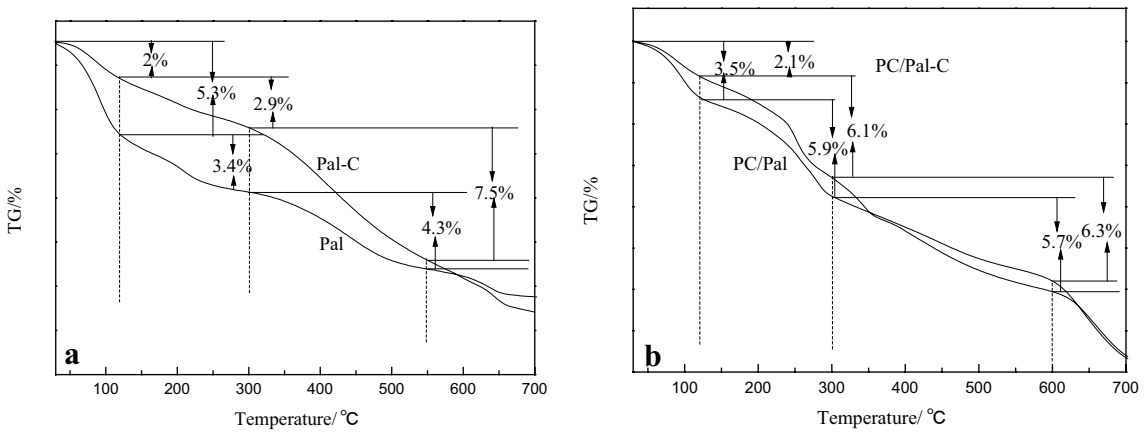

Fig. 1 TG curves of supports and catalysts **a** Pal and Pal-C; **b** PC/Pal and PC/Pal-C

range from 300 to 550 °C in our work, which is corresponding to the removal of the residual bound water and some structural hydroxyl water. The last step with a mass loss of 1.6% appears at above 550 °C, caused by loss of the remaining M-OH hydroxyl groups and the thermal decomposition of impurity [33–35]. For Pal-C, the mass losses in first and second steps are obviously lower than that in Pal, indicating the less content of adsorbed water and zeolitic water in Pal-C. This also suggests that the carbon modification reduces the hydrophilicity of Pal. However, the mass loss of Pal-C between 300 and 700 °C is higher than that in Pal, which can be assigned to the oxidative degradation of the carbonate species under air atmosphere. The above results further reveal that the sucrose-derived carbon has been successfully grafted onto the Pal, and the carbon modification can effectively improve the hydrophobicity of the Pal. For PC/Pal-C, the initial mass loss is obviously lower than that in PC/Pal, indicating the less content of adsorbed water in PC/Pal-C. In addition, the total mass loss of second and third steps of catalysts are higher than that of supports, which can be ascribed to the decomposition of $Cu_2Cl(OH)_3$ (will be presented in XRD) and the mass loss of carbon species.

3.2 XRD Analysis

Figure 2 shows the typical XRD patterns of Pal, Pal-C, PC/Pal and PC/Pal-C. The 110 plane of Pal at $2\theta = 8.4°$ ($d_{110} = 1.045$ nm) is attributed to the basal space of the Pal framework [36]. The diffraction peaks at $2\theta = 19.7°$ and 20.7° are assigned to the Si–O–Si crystalline layers in the Pal [29]. In addition, the reflection located at $2\theta = 26.6°$ indicates that there are quartz impurities existing in Pal [19].

Compared with Pal, the reflections at $2\theta = 16.3°$ (011), 17.6° (101), 32.4° (013) and 39.5° (220), characterization of $Cu_2Cl(OH)_3$ structure (JCPDS-#25-1427), are observed in the patterns of PC/Pal, and the reflections at $2\theta = 35.5°$ (022), 38.7° (111) are consistent with the data of the JCPDS file of CuO (JCPDS-#44–0706). The other reflections on the XRD pattern of PC/Pal correspond to palygorskite. Apparently, the Cu species on PC/Pal-C possesses the same phase as that on PC/Pal, and no other reflections of Cu species are detected. However, the intensities of $Cu_2Cl(OH)_3$ reflections on PC/Pal-C are lower than those on PC/Pal, on the contrary, the intensities of CuO reflections on PC/Pal-C are higher than that on PC/Pal. According to the Scherrer equation, the crystallite sizes of $Cu_2Cl(OH)_3$ on PC/Pal and PC/Pal-C are 39 and 31.8 nm, respectively. These are likely to suggest that the content of $Cu_2Cl(OH)_3$ is low or that $Cu_2Cl(OH)_3$ possesses a higher dispersion degree in PC/Pal-C. Wang et al. [37] claimed the Pd–Cu/MO_x ($MO_x = TiO_2$ and Al_2O_3) exhibited the excellent catalytic performance of CO oxidation due to the presence of $Cu_2Cl(OH)_3$. Thus, when the Pd loading was fixed, the higher dispersion of $Cu_2Cl(OH)_3$, the higher its catalytic activity would be, which is consistent with our experimental results. In addition, the absence of reflection of Pd species in both of the catalysts may indicate that the Pd species is highly dispersed on the supports or the size of Pd species is too small to be detected.

3.3 FT-IR Analysis

Figure 3 shows the FT-IR spectra of the PC/Pal, PC/Pal-C, Pal and Pal-C between 400 and 4000 cm^{-1}. In the FT-IR spectra of Pal and Pal-C, the sharp bands at 3618 and 3546 cm^{-1} and a broad band at 3500–3300 cm^{-1} are attributed to the stretching vibration of various –OH [26]. Compared with Pal, the band of –OH for Pal-C becomes smaller (inset, Fig. 3), which shows that the carbon modification could inhibit the water adsorption on the surface of the support. As a result, it is an effective method to promote

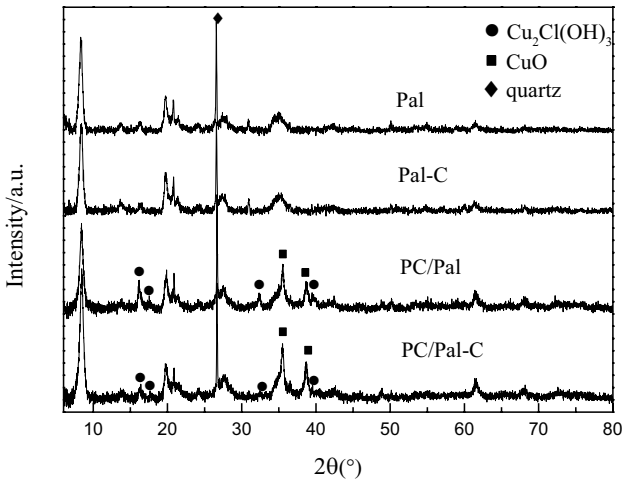

Fig. 2 XRD patterns of supports and catalysts

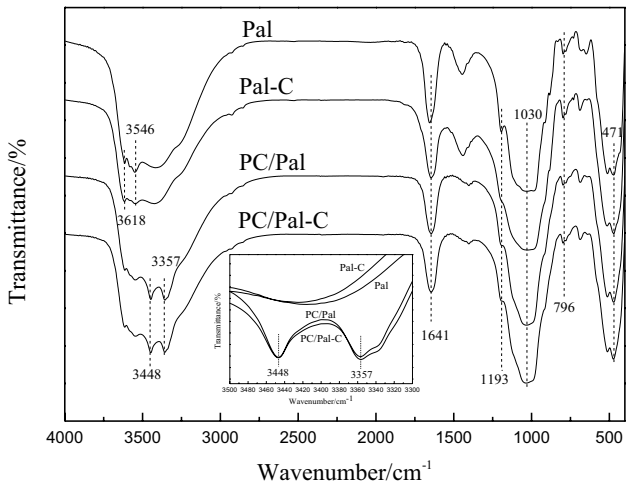

Fig. 3 FT-IR spectra of supports and catalysts

hydrophobicity of Pal by carbon modification. The band at 1641 cm^{-1} is brought about by the bending vibration of –OH. The bands at 1193, 1030 cm^{-1} are characteristic bands of palygorskite, corresponding to Si-O vibration and the in-layer Si–O band, respectively [38]. The band at 796 cm^{-1} indicates that there is quartz in the Pal, and the band at 471 cm^{-1} is due to Si–O–Si deformation vibration, which is consistent with the XRD results.

The bands of PC/Pal are similar to those of Pal, and the two bands of catalysts at 3448 and 3357 cm^{-1} are attributed to the –OH asymmetric and symmetric stretching modes of $Cu_2Cl(OH)_3$, respectively [39]. From the inset, it can be seen that the intensities of bands at 3448 and 3357 cm^{-1} have no significant difference in both of catalysts. Considering that FT-IR is not an effective quantitative analysis method, the amount of $Cu_2Cl(OH)_3$ on the PC/Pal and PC/Pal-C has been further calculated based on the results of H_2-TPR (will be shown soon).

3.4 BET and CA Analysis

The nitrogen adsorption–desorption isotherms of supports and catalysts are given in Fig. 4. The curves of all samples indicate that the adsorption isotherm exhibits a type III with H3-type hysteresis loop based on IUPAC classification. N_2 adsorption increases sharply at relatively pressure higher than 0.85, suggesting that the materials are mainly macropores [40].

The textual and surface properties and contact angles of supports and catalysts are listed in Table 1. It can be seen that the specific surface areas of Pal-C and PC/Pal-C slightly decrease after carbon modification, which may result from the deposition of carbon on the surface or in the channel of Pal. PC/Pal and PC/Pal-C show the nearly same pore diameter and pore volume. The changes of surface hydrophobicity of catalysts are also confirmed by water contact angle measurements. From Table 1, the contact angle of palygorskite increases after carbon modification. Furthermore, the PC/Pal-C, presenting an average contact angle of 26.9°, is more hydrophobic than PC/Pal, which has an average angle of 12.9°. As a result, carbon modification has little effect on the texture properties of the catalyst but slightly enhances surface hydrophobicity, which is in accordance with the results of TG analysis.

Table 1 Textural and surface properties and contact angles of supports and catalysts

Samples	BET (m^2/g)	Pore size (nm)	Pore volume (cm^3/g)	Contact angles (°)	
				L	R
Pal	135	8.0	0.27	22.0	22.2
Pal-C	103	10.6	0.27	38.6	43.2
PC/Pal	102	9.8	0.25	12.7	13.1
PC/Pal-C	90	9.7	0.22	26.8	27

3.5 H_2-TPR Analysis

The effects of carbon modification on the redox properties of the supports and catalysts were studied by H_2-TPR. The TPR profiles of the supports and catalysts are given in Fig. 5. As to the supports, a very broad and low peak occurs at nearly 500–650 °C, which implies the reduction of a small quantity of metal ions that contained in the palygorskite. The TPR profile of PC/Pal possesses three peaks, namely, α_1, β_1 and γ_1. According to literature [25], α_1 peak can be attributed to the co-reduction of Pd and highly dispersed $Cu_2Cl(OH)_3$. Combined with XRD and FT-IR results, peak β_1 at 218 °C can be ascribed to the reduction of microcrystalline $Cu_2Cl(OH)_3$ species contacting with the Pd species,

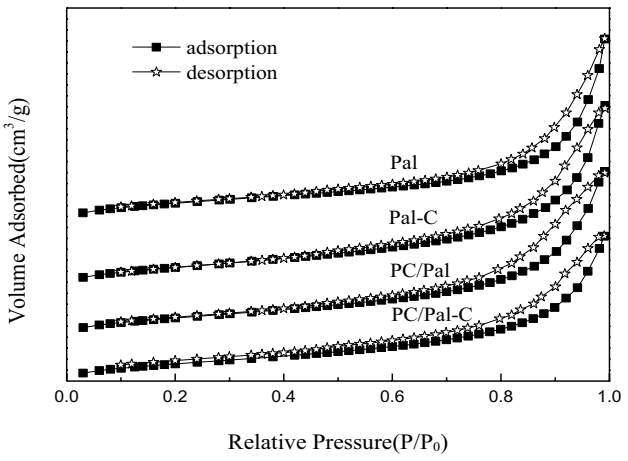

Fig. 4 N_2-physisorption isotherms of supports and catalysts

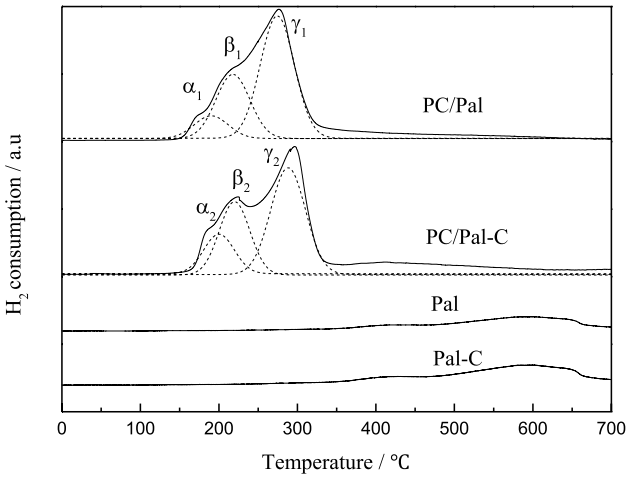

Fig. 5 TPR profiles of supports and catalysts

Table 2 Parameters of hydrogen consumption peaks of catalysts

	PC/Pal			PC/Pal-C		
	Peak α_1	Peak β_1	Peak γ_1	Peak α_2	Peak β_2	Peak γ_2
Temperature (°C)	192	218	274	196	220	280
Area	91	258	492	143	264	439
H_2 Consumption (μmol/g)	208.6	591.5	1127.8	327.7	605.2	1006.3
Total H_2 Consumption	1927.9			1939.2		

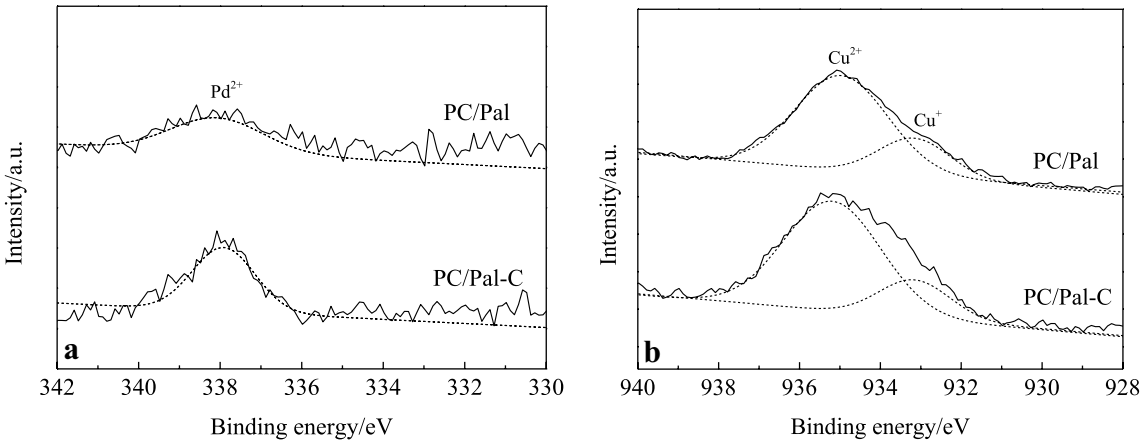

Fig. 6 XPS spectra of **a** Pd 3d and **b** Cu 2p for catalysts

and the γ_1 peak at 274 °C should be the reduction of crystal CuO. There are also three peaks in the TPR profile of the PC/Pal-C, α_2, β_2 and γ_2. Table 2 compares parameters of H_2 consumption peaks of PC/Pal with those of the PC/Pal-C. It can be seen that the total H_2 consumption of two catalysts are similar, and the reduction peak temperatures also have no distinct difference. However, compared with the H_2 consumption of peak α_1, the increased H_2 consumption of peak α_2 in PC/Pal-C is 119.1 μmol/g, which is far more than the theoretical H_2 consumption of Pd (32.89 μmol/g). This demonstrates that the larger area of peak α_2 can be mainly attributed to more highly dispersed $Cu_2Cl(OH)_3$. Moreover, the H_2 consumption of peak γ_2 is less than that of peak γ_1, indicating the amount of CuO species in PC/Pal-C decreases. Wang et al. [37] reported that the TPR profile of Pd–Cu/Al_2O_3 showed a negative peak at 300–400 K, which was ascribed to the decomposition of Pd β-hydride. However, the peak is absent in the catalysts due to the low Pd content.

3.6 XPS Analysis

Figure 6 depicts the XPS spectra of Pd and Cu species for the PC/Pal and PC/Pal-C. By fitting the Pd 3d XPS spectra of two catalysts (Fig. 6a), it can be seen that Pd species exists in the form of Pd^{2+} at 338.1 eV, which is considered to be the active Pd species for supported Wacker-type catalysts [24]. As shown in Fig. 6b, the Cu 2p XPS spectra of PC/Pal and PC/Pal-C present the Cu^+ (933.1 eV) and Cu^{2+} (935.0 eV) species. The Cu^{2+} species is deemed to be the active component to reoxide Pd^0 to Pd^{2+} [25]. Based on the area of their XPS peaks, the surface composition of two catalysts is quantified and shown in Table 3. As shown in Table 3, PC/Pal-C possesses higher $Cu^{2+}/(Cu^{2+}+Cu^+)$ ratio, which suggests that more surface Cu^{2+} species appears on the PC/Pal-C. Moreover, according to the peak areas of Pd^{2+} and Cu^{2+} and their sensitivity factors, the ratios of Pd^{2+}/Cu^{2+} in PC/Pal-C and PC/Pal are calculated. PC/Pal-C exhibits a larger Pd^{2+}/Cu^{2+} value (0.235) than PC/Pal (0.223). It indicates that more Pd^{2+} species exists on the surface of PC/Pal-C, which may contribute to the higher CO catalytic activity. As confirmed by the XRD and H_2-TPR results, the PC/Pal-C shows the more highly dispersed $Cu_2Cl(OH)_3$. The $Cu_2Cl(OH)_3$ species plays a vital role in the CO oxidation to improve the catalytic activity [41]. Therefore, the better catalytic performance of PC/

Table 3 Surface composition of catalysts obtained from XPS analysis

Samples	Pd^{2+}	Cu^{2+}	Cu^+	$Cu^{2+}/(Cu^{2+}+Cu^+)$	Pd^{2+}/Cu^{2+}
	Area			Area%	
PC/Pal	6094.2	36077.3	11311.4	76.1	0.223
PC/Pal-C	7929.3	44528.4	11115.0	80.0	0.235

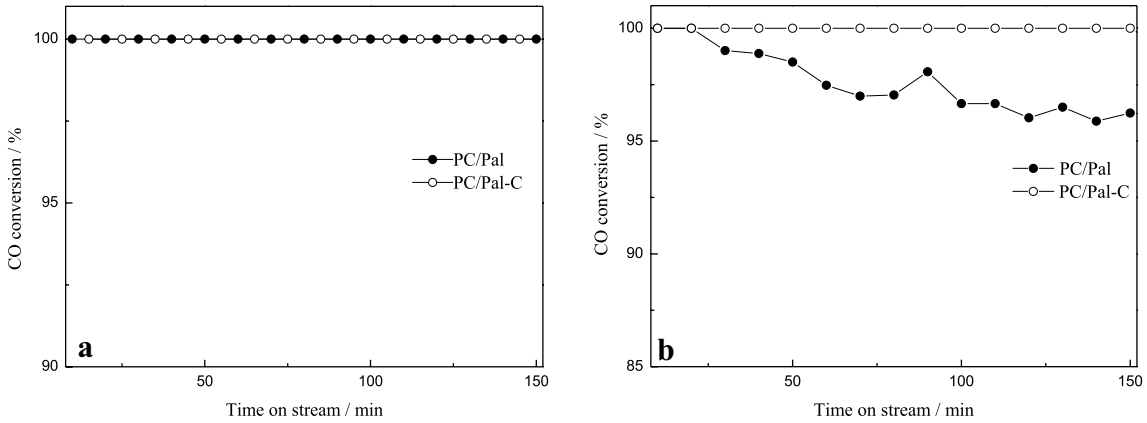

Fig. 7 Effects of moisture concentrations on the catalytic performance over catalystsReaction Conditions: 0.5% CO, GHSV 8000 h^{-1}, water vapor **a** 1.8 vol% **b** 3.3 vol%

Pal-C may be due to the more surface active Pd^{2+} and highly dispersed $Cu_2Cl(OH)_3$.

3.7 Catalytic Performance for Room-Temperature CO Oxidation Under Humid Circumstances

The effect of the moisture concentrations on the CO conversion over PC/Pal and PC/Pal-C was tested, and the catalytic performance of two catalysts is given in Fig. 7. From the Fig. 7a, it can be seen that the catalytic activities of PC/Pal and PC/Pal-C have no difference under the reaction conditions of 0.5 vol.% CO and 1.8 vol.% H_2O in the feed gas, and the CO conversions are almost as high as 100%. However, under the conditions of 0.5 vol.% CO and 3.3 vol.% H_2O (Fig. 7b), CO conversion over PC/Pal significantly decreases with the extension of reaction time, and CO conversion over PC/Pal-C still maintains at 100% at least 150 min. Further improving space velocity, it can be seen that the initial activity of PC/Pal is lower than that of PC/Pal-C (Figure S1). This demonstrates that the catalytic activity and stability of PC/Pal-C for room-temperature CO oxidation under moisture-rich conditions are obviously improved after the carbon modification of Pal. Continuing to increase the carbon content, the catalysts still exhibit favorable stability, but the poor catalytic activity (Figure S2).

A moderate amount of water is essential for the catalytic activity of the supported Wacker catalyst, as water molecules are involved in the catalytic cycle. However, aggregation and condensation of water molecules on the catalyst active sites leads to the decrease of catalytic activity when excess moisture is present in the feed gas. Such as the Wacker catalysts supported on Al_2O_3, the activity of $Pd–Cu–Cl_x/Al_2O_3$ is hardly varied for 30 h in ~ 1000 ppm moisture, however, in the presence of ~ 6000 ppm moisture, its activity decreases gradually with the reaction time due to the capillary condensation in hydrophilic alumina support [26]. In this paper, the PC/Pal-C exhibits not only higher catalytic activity, but also more excellent stability than the PC/Pal for room-temperature CO oxidation under moisture-rich conditions. On the basis of the XPS and H_2-TPR results, it can be concluded that the more active Pd^{2+} and highly dispersed $Cu_2Cl(OH)_3$ species present on the PC/Pal-C, which promotes the higher catalytic activity. The TG and CA results indicate that the slightly enhanced hydrophobicity of PC/Pal-C could properly restrain the moisture condensation on the catalyst surface, which may account for the excellent catalytic stability.

4 Conclusions

Pd-Cu/Palygorskite catalysts were prepared via a deposition precipitation method using Pal-C and Pal as supports, respectively. The catalytic activities toward CO oxidation at room temperature and in humid circumstances were investigated. It is found that PC/Pal-C exhibits more excellent catalytic performance than PC/Pal. The characterization results reveal that carbon modification leads to the more active Pd^{2+} and highly dispersed $Cu_2Cl(OH)_3$ species on the PC/Pal-C, which is beneficial for CO oxidation. In addition, the hydrophobicity of PC/Pal-C has been slightly increased after carbon modification, which may inhibit properly moisture condensation on the catalyst surface. The excellent catalytic performance of PC/Pal-C can be ascribed to the more surface active species and the proper hydrophobicity.

Acknowledgements Authors gratefully acknowledge the financial support from Shanxi provincial key research and development plan project (201603D121018-1); the National Natural Science Foundation of China (21673132); and the Key Laboratory of Applied Surface and Colloid Chemistry (Shaanxi Normal University).

Compliance with Ethical Standards

Conflict of interest On behalf of all authors, the corresponding author states that there is no conflict of interest.

References

1. Chen MS, Goodman DW (2004) Science 306:252
2. Su YF, Tang ZC, Han WL, Song Y, Lu GX (2015) Catal Surv Asia 19:68
3. Doggali P, Kusaba H, Einaga H, Bensaid S, Rayalu S, Teraoka Y, Labhsetwar N (2011) J Hazard Mater 186:796
4. Jiang HX, Wu XH, Wang CX, Huang P, Li YH, Zhang MH (2017) Catal Surv Asia 21:37
5. Freund HJ, Meijer G, Scheffler M, Schlögl R, Wolf M (2011) Angew Chem Int Ed 50:10064
6. Su YF, Dai LF, Zhang QW, Li YZ, Peng JX, Wu RA, Han WL, Tang ZC, Wang Y (2016) Catal Surv Asia 20:231
7. Gordon EB, Karabulin AV, Matyushenko VI, Sizov VD, Rostovshchikova TN, Nikolaev SA, Gurevich SA (2016) High Energy Chem 50:292
8. Zhu HQ, Qin ZF, Shan WJ, Shen WJ, Wang JG (2005) J Catal 233:41
9. He BB, Zhao QG, Zeng ZG, Wang XH, Han S (2015) J Mater Sci 50:6339
10. Yang Q, Du LY, Wang X, Jia CJ, Si R (2016) Chin J Catal 37:1331
11. Oxford SM, Henao JD, Yang JH, Kung MC, Kung HH (2008) Appl Catal A Gen 339:180
12. Li L, Wang AQ, Qiao BT, Lin J, Huang YQ, Wang XD, Zhang T (2013) J Catal 299:90
13. Wang GY, Lian HL, Zhang WX, Jiang DZ, Wu TH (2002) Kinet Catal 43:433
14. Kaplin IY, Lokteva ES, Golubina EV, Maslakov KI, Chernyak SA, Lunin VV (2017) Kinet Catal 58:585
15. Wang YZ, Zhao YX, Gao CG, Liu DS (2007) Catal Lett 116:136
16. Wang YZ, Zhao YX, Gao CG, Liu DS (2008) Catal Lett 125:134
17. Venkataswamy P, Jampaiah D, Mukherjee D, Aniz CU, Reddy BM (2016) Catal Lett 146:2105
18. Wang X, Zhong W, Li YW (2015) Catal Sci Technol 5:1014
19. Cao JL, Shao GS, Wang Y, Liu Y, Yuan ZY (2008) Catal Commun 9:2555
20. Jiang XY, Zhou RX, Yuan XX, Zheng XM, Jin SS (1996) J Environ Sci 8:145
21. Xie XW, Li Y, Liu ZQ, Haruta M, Shen WJ (2009) Nature 458:746
22. Wang L, Wang W, Zhang YH, Guo YL, Lu GX, Guo Y (2015) Catal Today 242:315
23. Shen YX, Guo Y, Wang L, Wang YQ, Guo YL, Guo YQ, Lu GZ (2011) Catal Sci Technol 1:1202
24. Shen YX, Lu GZ, Guo Y, Wang YQ, Guo YL, Gong XL (2011) Catal Today 175:558
25. Zhou FY, Du XX, Yu J, Mao DS, Lu GZ (2016) Rsc Adv 6:66553
26. Wang YZ, Fan LY, Shi J, Li X, Zhao YX (2015) Catal Lett 145:1429
27. Wang YZ, Li X, Lv TT, Wu RF, Zhao YX (2018) React Kinet Mech Cat 124:203
28. Wang YZ, Shi J, Wu RF, Li X, Zhao YX (2016) Appl Clay Sci 119:126
29. Wu XP, Zhu WY, Zhang XL, Chen TH, Frost RL (2011) Appl Clay Sci 52:400
30. Tian GY, Wang WB, Mu B, Kang YR, Wang AQ (2015) J Taiwan Inst Chem Eng 50:252
31. Zhang XL, Cheng LP, Wu XP, Tang YZ, Wu YC (2015) J Environ Sci 33:97
32. Wang H, Luo R, Ji S, Linkov V, Wang R (2014) Fuel Cells 14:42
33. Zhang Z, Wang WB, Wang AQ (2015) Appl Clay Sci 107:230
34. Cheng HF, Yang J, Frost RL (2011) Thermochim Acta 512:202
35. Liang XF, Xu YM, Tan X, Wang L, Sun YB, Lin DS, Sun Y, Qin X, Wang Q (2013) Colloids Surf A 426:98
36. Yang HM, Tang AD, Ouyang J, Li M, Mann S (2010) J Phys Chem B 114:2390
37. Wang FG, Zhang HJ, He DN (2014) Environ Technol 35:347
38. Wang YZ, Wang YN, Li X, Liu ZT, Zhao YX (2018) Environ Technol 39:780
39. Wei W, Gao P, Xie JM, Zong SK, Cui HL, Yue XJ (2013) J Solid State Chem 204:305
40. Yuan ZY, Ren TZ, Vantomme A, Su BL (2004) Chem Mater 16:5096
41. Wang FG, Zhao KF, Zhang HJ, Dong YM, Wang T, He DN (2014) Chem Eng J 242:10